Journal of Medicinal Chemistry

Article

pubs.acs.org/jmc

Modulating the Anticancer Activity of Ruthenium(II)−Arene Complexes

Catherine M. Clavel,[†] Emilia Păunescu,[†] Patrycja Nowak-Sliwinska,[†] Arjan W. Griffioen,[‡] Rosario Scopelliti,[†] and Paul J. Dyson*[,†]

[†]Institut des Sciences et Ingénierie Chimiques, Ecole Polytechnique Fédérale de Lausanne (EPFL), CH-1015 Lausanne, Switzerland

[‡]Angiogenesis Laboratory, Department of Medical Oncology, VUMC Cancer Center Amsterdam, 1081 HV Amsterdam, The Netherlands

Supporting Information

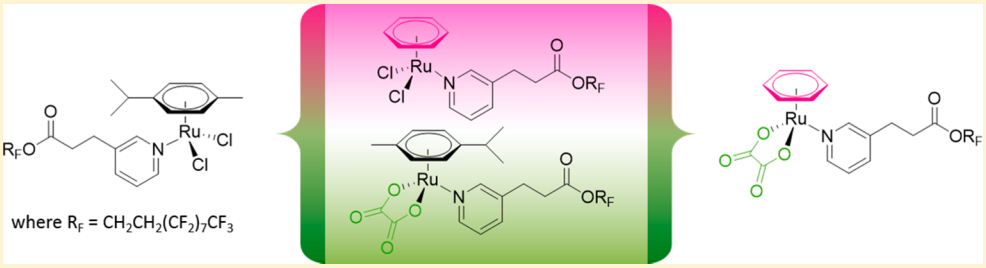

ABSTRACT: Following the identification of [Ru(η^6-*p*-cymene)Cl_2(1*H*,1*H*,2*H*,2*H*-perfluorodecyl-3-(pyridin-3-yl)propanoate)], a ruthenium(II)−arene complex with a perfluoroalkyl-modified ligand that displays remarkable in vitro cancer cell selectivity, a series of structurally related compounds were designed. In the new derivatives, the *p*-cymene ring and/or the chloride ligands are substituted by other ligands to modulate the steric bulk or aquation kinetics. The new compounds were evaluated in both in vitro (cytotoxicity and migration assays) and in vivo (chicken chorioallantoic membrane) models and were found to exhibit potent antivascular effects.

INTRODUCTION

Platinum-based drugs are widely applied in the clinic despite being limited by acquired or intrinsic resistance and severe side effects.[1,2] These problems emanate from the major target of cisplatin and related compounds, i.e., DNA,[3−5] which is ubiquitous in diseased and healthy cells. The low selectivity of platinum-based drugs[6] results in numerous "off-target" side effects, notably nephrotoxicity, neurotoxicity, neuropathy, myelosuppresion, thrombocytopenia, and neutropenia.[7−9] Today's requirement for safer drugs, i.e., for compounds with larger therapeutic windows, has stimulated research into platinum drug delivery strategies[10−12] and also into the exploration for anticancer compounds based on other metals.[13−16] Of the alternatives to platinum-based anticancer drugs, most progress has been made with agents based on ruthenium that tend to exhibit fewer side effects than platinum-based complexes,[17,18] possibly due, in part, to transferrin-mediated delivery to tumor sites.[19,20] Two ruthenium(III) complexes, NAMI-A (imidazolium *trans*-[tetrachloro-(dimethylsulfoxide)imidazole ruthenium(III)]), which acts on solid metastatic tumors,[21] and KP1019 (indazolium *trans*-[tetrachlorobis(1*H*-indazole)ruthenium(III)]), which is effective against resistant tumors,[22] completed phase I and II clinical trials.[23] In addition to ruthenium(III) complexes, ruthenium(II)−arene complexes show considerable promise and they tend to be somewhat more stable than the ruthenium(III) complexes undergoing clinical evaluation.[24] Moreover, it is suggested that ruthenium(III) is activated by reduction to ruthenium(II) in situ.[25,26] Of the various ruthenium(II)−arene compounds studied,[27] those with the general structure [Ru(η^6-arene)X_2(PTA)] (PTA = 1,3,5-triaza-7-phosphaadamantane), the lead compound being RAPTA-C (shown in Figure 1),

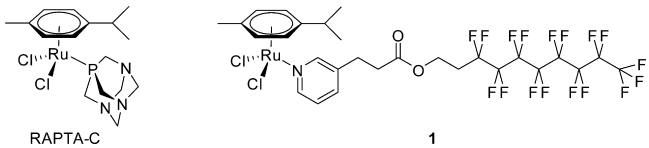

Figure 1. Chemical structures of the ruthenium(II)-*p*-cymene complexes RAPTA-C and **1**.

exhibit generally low cytotoxicity in vitro[28,29] but relevant antimetastatic[29−31] and antiangiogenic[32] properties in vivo. Moreover, it has recently been shown that RAPTA-C reduces the growth of primary tumors in preclinical models for ovarian and colorectal carcinomas via an antiangiogenic mechanism.[17] Although the full mechanism of action of the RAPTA class of compounds is not known,[33] contrary to classical platinum-based anticancer agents, RAPTA-C binds to the histone protein

Received: October 28, 2014
Published: March 26, 2015

DOI: 10.1021/jm501655t
J. Med. Chem. 2015, 58, 3356−3365

Scheme 1. Structures of the Newly-Synthesized Derivatives of 1

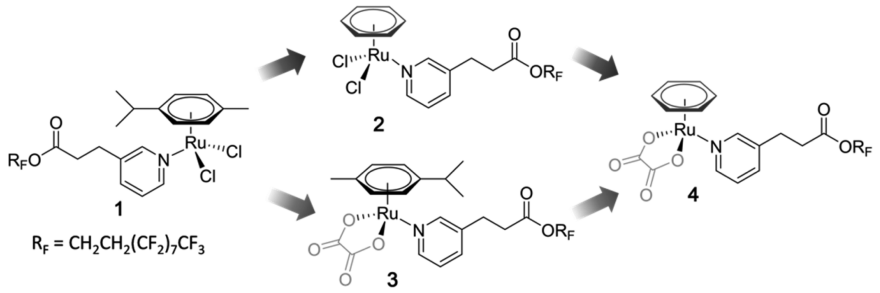

core in chromatin and not to the DNA.[33−35] It has also been shown that histone interactions can lead to antiangiogenic activity.[36,37]

Despite the promising pharmacological properties of ruthenium(II)−arene compounds, further enhancing their efficacy and selectivity in vivo is important. Various characteristics of the tumor environment or targeting strategies have been exploited in this purpose. For example, compounds that are activated by differences between the tumor tissue and the surrounding normal tissue, such as the lower oxygen content and lower pH, have been developed,[38−40] and attachment of ruthenium complexes to macromolecules results in selective permeability of the tumor vasculature via the enhanced permeation and retention effect.[41,42] Examples of macromolecular systems containing multiple ruthenium(II)−arene units include dendrimeric architectures,[43−45] multinuclear ruthenium metallacycles or metallacages, and RAPTA-modified polymer or copolymer conjugates.[46−49]

The in vitro activation of ruthenium(II)−arene complexes derivatized with perfluorinated phosphine ligands that display modest thermoresponsive activation has been reported.[50] More recently, the structure of these compounds was modified to give compounds that, upon application of controlled mild hyperthermia from an external source, exhibit remarkable and selective cytotoxicity.[51] In contrast, the introduction of lipophilic chains on ruthenium(II)−arene complexes, via modification of a PTA,[52] imidazole,[53] or isonicotinic ester[54,55] ligands, leads to increased antiproliferative activity, presumably due to increased cell uptake, but not necessarily to increased cancer cell selectivity. The nature of the lipophilic chain, i.e., alkyl or perfluoroalkyl, and the length of the chain have a strong influence on cytotoxicity.[51] From a large series of derivatives, **1** (see Figure 1) was identified as a lead compound, displaying antiproliferative activity against four cancer cell lines (25−45 μM) and without any cytotoxic effect against nontumoral cells.[51,56] Moreover, evaluation of **1** in vivo in a xenografted ovarian carcinoma tumor (A2780) grown on the CAM led to a 90% reduction in the tumor growth.

Compound **1** is a promising drug lead in which the perfluoroalkyl chain appears to be essential for both drug activity and selectivity.[56] Herein, we describe new derivatives in which the *p*-cymene and/or the chloride ligands are replaced by other ligands (Scheme 1), bringing more versatility to this new class of selective anticancer complexes. The new structures have been evaluated in both in vitro and in vivo models.

RESULTS AND DISCUSSION

Complex **2**, in which the *p*-cymene ring in **1** is replaced by a benzene ring, was prepared in high yield from the reaction of ligand **L**[51] with the corresponding benzene dimer in dichloromethane at room temperature (Scheme 2). Benzene was chosen, as previous reports indicated that a less bulky arene could enhance cell uptake and antiproliferative activity.[29,57−59]

Scheme 2. Synthesis of 2

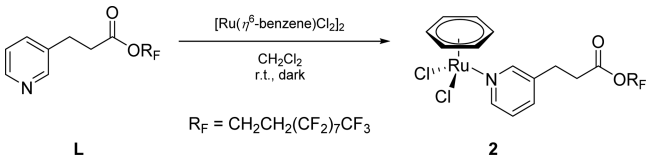

Cisplatin and ruthenium(II)−arene complexes undergo activation by hydrolysis[29,60] with the hydrolysis rate and stability altered by substituting the chloride ligands by oxalates, i.e., as in oxaliplatin and carboplatin,[61,62] and the ruthenium compounds oxalo-RAPTA-C, carbo-RAPTA-C,[28] and other ruthenium−arene systems.[28,63−65] The two chloride ligands in **1** and **2** were replaced by an oxalate ligand using a synthetic route adapted from a literature procedure[28] as shown in Scheme 3. The appropriate ruthenium dimer was reacted with

Scheme 3. Synthesis of 3 and 4

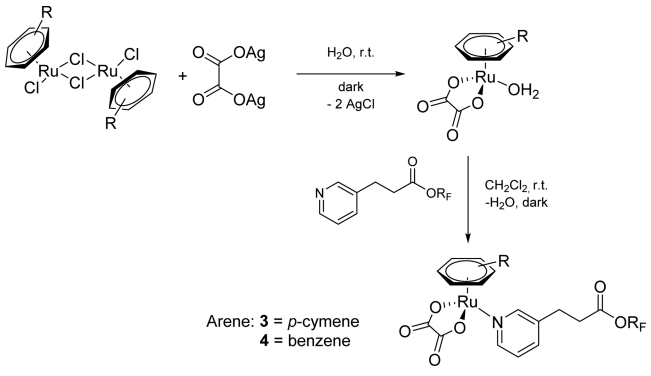

silver oxalate to give the intermediate species, [Ru(η^6-arene)(oxalate)(H_2O)], which subsequently reacts with ligand **L** to afford the desired complexes, **3** and **4**, in good yield.

Compounds **2**−**4** were fully characterized by ^{1}H, ^{13}C, and ^{19}F NMR spectroscopy, ESI mass spectrometry, IR spectroscopy, and elemental analysis (see Experimental Section). The formation of **2** could be easily monitored and confirmed by NMR spectroscopy. As previously described for **1**,[51] complexation of the modified pyridine ligand to the ruthenium(II)−benzene unit via the pyridine N atom in **2** is accompanied by a change to higher frequency of the peaks of the pyridine protons in the α position to the nitrogen atom ($\Delta\delta_H \approx 0.5$ ppm) and the respective carbon atoms ($\Delta\delta_C \approx 5$ ppm). The six protons

DOI: 10.1021/jm501655t
J. Med. Chem. 2015, 58, 3356−3365

of the benzene ring in complex **2** appear as a singlet at 5.65 ppm in the ^{1}H NMR spectrum, and the corresponding six carbon atoms give rise to a signal at 84.5 ppm in the ^{13}C NMR spectrum. For the oxalate complex **3**, the peaks corresponding to the hydrogen and carbon atoms in the α position of the pyridine move to lower frequency relative to **1**.[51] In the ^{13}C NMR spectra of **3** and **4**, the coordinated oxalate ligand shows a characteristic peak at ∼165 ppm and the propionate peak is observed at ∼172 ppm. In **4**, the peaks corresponding to the hydrogen and carbon atoms in the α position of the pyridine also move to lower frequency compared to the analogous peaks in **2**. The ^{19}F NMR spectra of in **2**−**4** contain the peaks expected for the long perfluorinated chain present. The IR spectra of **2**−**4** contain a peak at ∼1740 cm^{-1}, confirming the presence of the propionate ester group in the ligand with additional peaks around 1645−1700 cm^{-1} attributable to the oxalate ligand. The ESI mass spectrum of **2** is dominated by species assigned to the $[M - Cl]^+$ ion, whereas the peak of highest relative intensity for **3** and **4** corresponds to the $[M + H]^+$ ions.

Crystals of **2** suitable for X-ray diffraction analysis were obtained from dichloromethane−chloroform. The structure of **2** is shown in Figure 2 with key bond parameters listed in Table 1. The complex adopts the familiar half-sandwich three-legged piano-stool geometry with the η^6-benzene ring forming the seat and the pyridine and two chloride ligands the legs of the stool. The bond parameters around the Ru center are remarkably similar to RAPTA-C[66] and the model complex Ru(η^6-*p*-cymene)Cl$_2$(methyl-3-(pyridin-3-yl)propanoate) **A** (see Table 1).[56] In the crystal, the carboxyl group and perfluorinated chain are almost coplanar, with a zigzag distribution of the carbon atoms of the perfluorinated chain in the same plane and the fluorine atoms being distributed symmetrically on both sides of the plane.

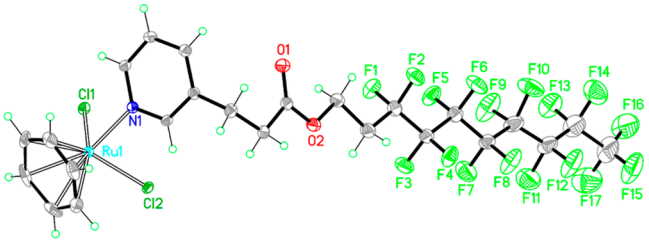

Figure 2. ORTEP representation of **2**. Thermal ellipsoids are 30% equiprobability envelopes, and H atoms are spheres of arbitrary diameter.

An interesting difference between **2** and **A** is the value of the torsion angles for the propionic side chain C_{py}−C−C−C(=O)O and C−C−C(=O)O−C (see Table 1), which in **2** is presumably influenced by the presence of the perfluorinated chain. Notably, the structural features determined for **2** are similar to those of another analogue with a shorter perfluorinated chain ($CH_2CH_2(CF_2)_5CF_3$) bearing a toluene ring instead of the benzene arene (see Supporting Information, data for complex **S1**).

In Vitro Studies. The antiproliferative activity of **2**−**4** was evaluated against human ovarian cancer cells (A2780), metastatic breast adenocarcinoma cells (MDA-MB-231), noncancerous embryonic kidney cells (HEK-293), immortalized endothelial cells (ECRF24), and primary human umbilical cord vein endothelial cells (HUVEC). Cytotoxicity was determined after 72 h using the MTT assay (see Table 2). Compounds **2** and **3** are more cytotoxic to the A2780 cancer cells than **1**, whereas **2**−**4** are less cytotoxic than **1** to the endothelial cells ECRF24 or HUVEC. Importantly, none of the compounds inhibit the growth of the HEK-293 cells at the maximum dose tested.

Table 2. IC$_{50}$ Values of 1−4 against A2780, MDA-MB-231, HEK-293, ECRF24, and HUVEC Cells after a 72 h Incubation Using the MTT Assay[a]

compd	A2780 (μM)	MDA-MB-231 (μM)	HEK-293 (μM)	ECRF24 (μM)	HUVEC (μM)
1	44 ± 1[51]	36 ± 2[51]	>100[51]	56 ± 4	>100
2	18.5 ± 0.3	>100	>100	>100	>100
3	22.4 ± 0.1	>100	>100	80 ± 4	>100
4	73 ± 6	>100	>100	>100	>100

[a]Errors represent the standard deviations.

Complex **2** is more cytotoxic to A2780 cells than **1** (IC$_{50}$ = 18.5 and 44 μM, respectively), while remaining nontoxic to noncancerous cells (IC$_{50}$ > 100 μM). In parallel, **3** is also more cytotoxic to A2780 cells than **1** (IC$_{50}$ = 22.4 μM). RAPTA-C has little effect on immortalized human endothelial (ECRF24)[32] cells, whereas **1** has an IC$_{50}$ value of 56 μM.

Table 1. Comparison of Key Bond Lengths (Å) and Angles (deg) in RAPTA-C, 2 and A[a]

	RAPTA-C[66]	**2**	**A**[56]
Ru-η^6	1.692, 1.701	1.662, 1.663	1.669(2)
Ru−P	2.296(2), 2.298(3)		
Ru−N		2.121(4), 2.125(4)	2.112(4)
Ru−Cl$_{ave}$	2.421, 2.426	2.415	2.4138(12)
Cl−Ru−Cl	87.25(8), 88.97(9)	88.25(4), 88.64(4)	87.64(4)
P−Ru−Cl$_{ave}$	84.01, 85.26		
N−Ru−Cl$_{ave}$		86.72, 86.47	85.22(11)
C_{py}−C−C−C(=O)O		66.3(7), −71.0(9)	178.22
C−C−C(=O)−O		−176.8(5), 174.4(7)	−26.45
C−C(=O)−O−C		178.9(6), 179.4(10)	−179.50

[a]In the case of RAPTA-C, there are two independent molecules in the asymmetric unit. The structure of complex **A**, Ru(η^6-*p*-cymene)Cl$_2$(methyl-3-(pyridin-3-yl)propanoate), is 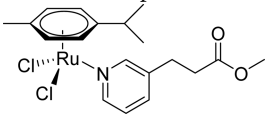

DOI: 10.1021/jm501655t
J. Med. Chem. 2015, 58, 3356−3365

Complexes **2**–**4** are less cytotoxic to immortalized ECRF24 cells than **1** with IC_{50} values of >100, 80, and >100 μM, respectively, and showed no significant activity at doses below 100 μM toward freshly isolated HUVEC cells.

Cellular uptake of **1** and **2** in A2780 cells was determined after a 24 h incubation with RAPTA-C included in the study as a reference compound. The level of accumulation of **1** and **2** in the A2780 cells is very similar and is approximately 3-fold higher than that observed for RAPTA-C (Figure 3) and correlates well with the differences in cytotoxicities of the compounds against this cell line.

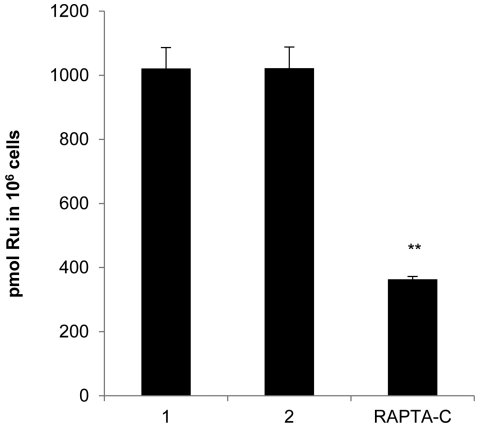

Figure 3. Intracellular uptake of **1**, **2**, and RAPTA-C (pmol/10^6 cells) in A2780 cells after a 24 h incubation: (**) p = 0.00181 (one-way ANOVA) (dose, 250 μM). Error bars correspond to standard deviations.

The effect of **2**–**4** on the migration of invasive breast cancer MDA-MB-231 and immortalized endothelial ECRF24 cells was assessed using a scratch assay by evaluating the extent of wound closure after incubation of the cells with the compounds at various doses.[67] Following a 14 h incubation, approximately 20% inhibition of MDA-MB-231 cell mobility was observed for **2**–**4** at a concentration of 50 μM (Figure 4). Since the duplication time for this cell line is 38 h, cell proliferation is unlikely to significantly influence the inhibition of migration. Overall antimigration and antiproliferation activity of complexes **2**–**4** in this cell line is relatively low, which is not unexpected as this cell line is known to show only a modest response to chemotherapeutic agents.[68] Similar experiments could not be conducted on A2780 cells, as they do not migrate. At the same dose, **1** inhibits MDA-MB-231 cell mobility by 50%, which is comparable to the activity of sunitinib, a clinically used anticancer compound.[56] Hence, the structural modifications in complexes **2**–**4** do not lead to more efficient cell migration inhibition than **1**. Furthermore, none of the complexes significantly inhibit the migration of ECRF24 cells.

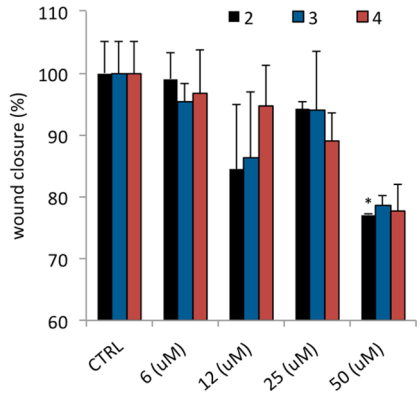

Figure 4. Assessment of migration inhibition of MDA-MB-231 cells after exposure to **2**, **3**, and **4**: wound closure in MDA-MB-231 cultures after a 14 h incubation with complexes at doses ranging between 6 and 50 μM; 0.1% DMSO in 0.9% NaCl as a control. Error bars represent the standard error of the mean: (*) p = 0.05 (paired t-test).

To elucidate the mechanism of cell death DNA, profiles of propidium iodide stained A2780, MDA-MB-231, and HUVEC cells treated with **2**–**4** were analyzed by FACS (Table 3).[69]

Table 3. Apoptosis Induction (%) and Cell Cycle Phases (%) Evaluated in A2780, MDA-MB-231, and HUVEC Cells Using FACS Analysis of PI-Stained Cells[a]

cell type	compound	apoptosis	G0/G1 + S	G2/M
A2780	control	2.5	38.9	12.9
	2	27.1	33.3	11.2
	3	38.1	29.6	8.3
	4	35.0	30.0	7.9
MDA-MB-231	control	1.3	64.5	15.7
	2	1.7	60.8	12.3
	3	3.2	62.5	13.2
	4	1.2	66.3	14.9
HUVEC	control	1.3	64.5	15.7
	2	1.7	60.8	12.3
	3	3.2	62.5	13.2
	4	1.2	66.3	9.5

[a]Measurements were performed after a 24 h incubation with **2**–**4** at their respective IC_{50} concentrations in A2780 cells and at a concentration of 50 μM in MDA-MB-231 and HUVEC cells.

Compounds **2**–**4** induced apoptosis in A2780 cells, assessed by the number of subdiploid cells, in a range 27.1–38.1% at their IC_{50} concentration for the A2780 cell line and at a concentration of 50 μM in the other cell lines screened. For **1**, only a moderate induction of apoptosis was observed in A2780 cells,[56] in good agreement with other studies reporting apoptosis-based cell death by ruthenium complexes.[32,69] No significant changes in the cell cycle were observed for **2**–**4**, whereas **1** was shown to synchronize cells in the G2/M phase.[56] A small induction of apoptosis (almost 2-fold higher compared to control) was observed for **3** in MDA-MB-231 and HUVEC cells.

In Vivo Activity in the Chicken Chorioallantoic Model. Since antiproliferative activity in activated human endothelial cells (ECRF24) was observed in the absence of toxicity to HEK-293 cells (Table 2), the antiangiogenic activity of **2**–**4** was tested in vivo using the chicken chorioallantoic membrane (CAM) model.[70] Compounds **2**–**4** were administered via a daily intravenous (iv) injection between embryo development days (EDDs) 11 and 14 (Figure 5A), followed by in ovo imaging of the CAM vasculature on EDD 15 using FITC–dextran (fluorescein isothiocyanate–dextran 20 kDa, 20 μL, 25 mg/mL, Sigma-Aldrich) epi-fluorescence angiography, and subsequent analysis by the image-processing quantification method.[71] Intravenous administration of **2**–**4** at a dose of 50 μM (corresponding to 0.45 mg kg^{-1} day^{-1} for **2**, 0.52 mg kg^{-1} day^{-1} for **3**, or 0.48 mg kg^{-1} day^{-1} for **4**) induced an antivascular effect represented by a decrease in the number of

DOI: 10.1021/jm501655t
J. Med. Chem. 2015, 58, 3356–3365

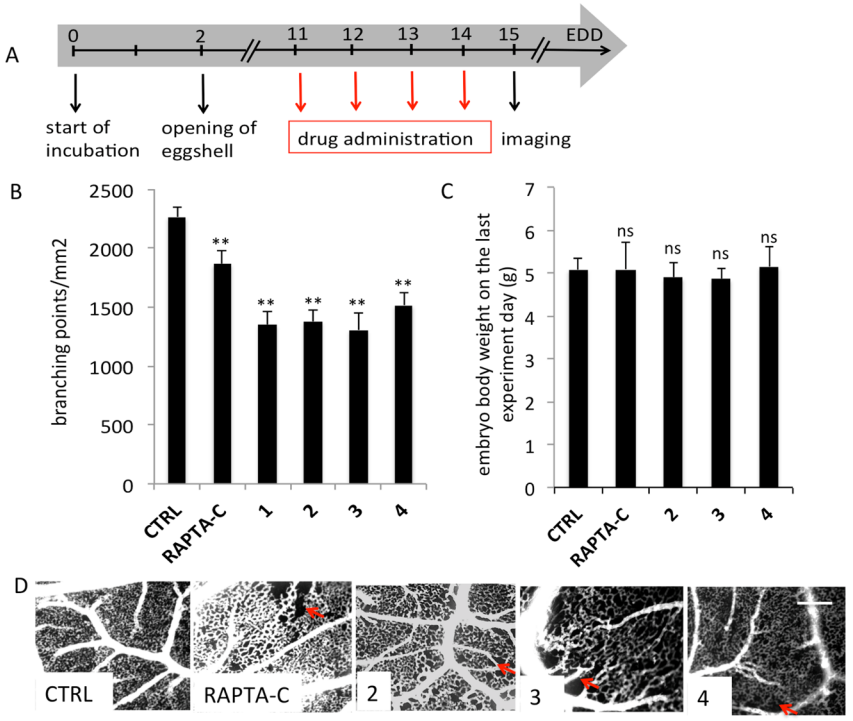

Figure 5. Antivascular effects in the CAM model. Results were obtained in the CAM after iv administration of **1**−**4** or RAPTA-C (50 μM) between 11 and 14 embryo development day (1 injection/day for 4 days, A). (B) Quantification of digital analysis of the fluorescence angiography images: number of branching points (mm^2). All points are statistically significant with (**) $p < 0.01$ (*t*-test). (C) Embryo body weight comparison at the last experiment day. Error bars represent the standard error of the mean. (D) The vasculature is visualized by FITC−dextran fluorescence angiography (20 kDa, 25 mg/kg, λ_{ex} = 470 ± 20 nm, λ_{em} > 520 nm). Scale bar: 100 μm. Red arrows indicate avascular zones.

branching points/mm^2 on the CAM capillary bed compared to the controls (0.1% DMSO in 0.9% NaCl; 2264 ± 87). For all complexes, treatment resulted in a decrease of branching points/mm^2 to 1378 ± 100 (**2**, ***$p = 1.66 \times 10^{-6}$), 1305 ± 146 (**3**, ***$p = 4.66 \times 10^{-6}$), and 1516 ± 104 (**4**, ***$p = 1.53 \times 10^{-6}$), compared to 1349 ± 113 for **1** (***$p = 2.89 \times 10^{-5}$). Interestingly, these effects were significantly more pronounced (with *p = 0.018 for **2**, **p = 0.001 for **3**, and **p = 0.005 for **4**) than those observed for RAPTA-C (1868 ± 110, **p = 0.008 vs control; see Figure 5B). Note that previously a 50 μM dose of **1** was found to reduce branching points by 26.3% compared to the control, somewhat less than observed here but a difference that is not unexpected with the CAM model.[56] No significant loss of embryo body weight was observed, suggesting a lack of toxicity to the embryo at the tested concentrations (Figure 5C). Representative fluorescence angiographies for the control and **2**−**4** are presented in Figure 5D. Arrows indicate avascular zones, represented by the lack of FITC−dextran fluorescence. The avascular zones observed may be due to antiangiogenic activity or a lack of vascular perfusion resulting from thrombosis. The reduced number of branching points for **2**−**4** was comparable to the effect of **1**, as well as RAPTA-C. The embryo body weight was not influenced by treatment of **2**−**4** or RAPTA-C (Figure 5C). In comparison, the ruthenium(III) antimetastatic complex NAMI-A also exhibits an antiangiogenic effect even if not per se but due to the presence of VEGF in the in vivo rabbit cornea assay.[72] In the CAM-sponge model, NAMI-A at concentrations of 120 and 240 μM was shown to reduce the number of vessels.[73]

In summary, a series of related ruthenium(II)−arene compounds were prepared that exhibit more selective cytotoxicity to A2780 cancer cells and inhibit the migration of MDA-MB-231 tumor cells in the absence of an effect on endothelial cells. Moreover, these compounds display a stronger antivascular effect in the in vivo chicken chorioallantoic membrane model than RAPTA-C, which is known to inhibit tumor growth via an antiangiogenic mechanism.[51]

EXPERIMENTAL SECTION

All chemicals were purchased from commercial sources (Aldrich, AlfaAesar, and Acros Chemicals) and used without further purification. The reactions were performed in solvents dried using a dry-column apparatus and collected and used under inert atmosphere of N_2. The dimer $[Ru(\eta^6\text{-benzene})Cl_2]_2$, **1**, the corresponding ligand, and silver oxalate were prepared and purified according to literature procedures.[28,51,74] Reactions were performed under inert atmosphere of N_2 using Schlenk techniques, and the complexation reactions and manipulation of the ruthenium dimers and complexes were performed in the absence of light. ^{1}H (400.13 MHz), ^{19}F (376.46 MHz), and ^{13}C (100.62 MHz) NMR spectra were recorded on a Bruker Avance II 400 spectrometer at 298 K. Chemical shifts are reported in parts per million (ppm) and referenced to deuterated solvent residual peaks ($CDCl_3$, ^{1}H δ 7.26, $^{13}C\{^1H\}$a δ 77.16 ppm; CD_2Cl_2, ^{1}H δ 5.32, $^{13}C\{^1H\}$ δ 53.84 ppm),[75] and coupling constants (J) are reported in hertz (Hz). IR spectra were recorded on a PerkinElmer Spectrum One FT-IR spectrometer at room temperature. Electrospray ionization mass spectra were obtained on a Thermo-Finnigan LCQ Deca XP Plus quadropole ion-trap instrument operated in positive-ion mode. Elemental analysis was carried out by the microanalytical laboratory at the Institute of Chemical Sciences and Engineering (EPFL). Elemental analysis data confirm ≥96% purity for all the tested compounds. Melting points were determined using a SMP3 Stuart melting point apparatus and are uncorrected.

$[Ru(\eta^6$-benzene)Cl_2(1*H*,1*H*,2*H*,2*H*-perfluorodecyl-3-(pyridin-3-yl)propanoate)] 2. To a suspension of $[Ru(\eta^6\text{-benzene})Cl_2]_2$ (0.180 g, 0.359 mmol, 1 equiv) in dichloromethane (10 mL) a solution of 1*H*,1*H*,2*H*,2*H*-perfluorodecyl-3-(pyridin-3-yl)propanoate **L**

DOI: 10.1021/jm501655t
J. Med. Chem. 2015, 58, 3356−3365

(0.450 g, 0.753 mmol, 2.1 equiv) in CH_2Cl_2 (30 mL) was added dropwise. The reaction mixture was stirred at room temperature for 72 h. The reaction mixture was filtered, and the filtrate was concentrated under reduced pressure almost to dryness. The product was precipitated with Et_2O (5 mL) followed by successive washing of the obtained orange solid with Et_2O (3 × 20 mL), hexane (20 mL), and Et_2O (20 mL). The orange solid was recovered by filtration and dried under a flow of N_2 and then under high vacuum to afford an orange solid (0.577 g, η = 95%). Mp (°C) = 177.5−178.5. ^{1}H NMR ($CDCl_3$, 318 K) δ_H, ppm: 9.00 (1H, s, N_{py}-C$\underline{H}$-C), 8.97 (1H, d, N_{py}-C$\underline{H}$-CH, $^3J_{H,H}$ = 5.5 Hz), 7.61 (1H, d, N_{py}-CH−C-C$\underline{H}$, $^3J_{H,H}$ = 7.4 Hz), 7.24 (1H, dd overlapped, N_{py}-CH-C$\underline{H}$, $^3J_{H,H}$ = 7.4 Hz), 5.65 (6H, s, 6 × CH(*Ar*)), 4.40 (2H, t, O-C$\underline{H_2}$-CH$_2$, $^3J_{H,H}$ = 6.5 Hz), 2.97 (2H, t, *Py*-C$\underline{H_2}$-CH$_2$-C═O, $^3J_{H,H}$ = 7.3 Hz), 2.68 (2H, t, *Py*-CH$_2$-C$\underline{H_2}$-C═O, $^3J_{H,H}$ = 7.3 Hz), 2.42−2.54 (2H, m, O-CH$_2$-C$\underline{H_2}$). ^{13}C NMR ($CDCl_3$, 318 K) δ_C, ppm: 171.5 (1C, CH$_2$-$\underline{C}$═O), 155.1 (1C, N_{py}-$\underline{C}$H-C), 153.2 (1C, N_{py}-$\underline{C}$H-CH), 137.8 (1C, N_{py}-CH-C-$\underline{C}$H), 137.0 (1C, N_{py}-CH-$\underline{C}$-CH), 124.1 (1C, N_{py}-CH-$\underline{C}$H), 107.6−120.1 (8C, series of multiplets, CH$_2$-$\underline{C}$F$_2$-CF$_2$, CH$_2$-CF$_2$-$\underline{C}$F$_2$, CH$_2$-(CF$_2$)$_2$-$\underline{C}$F$_2$, CH$_2$-(CF$_2$)$_3$-$\underline{C}$F$_2$, $\underline{C}$F$_2$-(CF$_2$)$_2$-CF$_3$, $\underline{C}$F$_2$-CF$_2$-CF$_3$, CF$_2$-$\underline{C}$F$_2$-CF$_3$, CF$_2$-CF$_2$-$\underline{C}$F$_3$), 84.5 (6C, 6 × $\underline{C}$H(*Ar*)), 56.7 (1C, t, O-$\underline{C}$H$_2$-CH$_2$, $^3J_{C,F}$ = 4 Hz), 34.5 (1C, *Py*-CH$_2$-$\underline{C}$H$_2$-C═O), 30.6 (1C, t, O-CH$_2$-$\underline{C}$H$_2$, $^2J_{C,F}$ = 22 Hz), 27.6 (1C, *Py*-$\underline{C}$H$_2$-CH$_2$-C═O). ^{19}F NMR ($CDCl_3$, 318 K) δ_F, ppm: −80.77 (3F, t, C$\underline{F_3}$, $^3J_{F,F}$ = 9.8 Hz), −113.40 (2F, m, CH$_2$-C$\underline{F_2}$-CF$_2$), −121.42 (2F, m, CH$_2$-(CF$_2$)$_2$-C$\underline{F_2}$), −121.68 (4F, m, CH$_2$-(CF$_2$)$_3$-C$\underline{F_2}$, CH$_2$-(CF$_2$)$_4$-C$\underline{F_2}$), −122.50 (2F, m, C$\underline{F_2}$-CF$_2$-CF$_3$), −123.35 (2F, m, CH$_2$-CF$_2$-C$\underline{F_2}$), −125.91 (2F, m, C$\underline{F_2}$-CF$_3$). IR (ν, cm^{-1}): 3038, 2931 (CH-*Ar*, CH$_2$, CH, CH$_3$), 1741 (C═O), 1475−1434 (*Py* C═C, C═N), 1368, 1330, 1244−1115 (CF$_2$, CF$_3$), 1197 (C−O). ESI-MS(+): *m*/*z* found 811.9855 [M − Cl]$^+$, calcd for $C_{24}H_{18}ClF_{17}NO_2Ru$ 811.90; the experimental isotopic pattern fits well the calculated one. Anal. (%) Calcd for $C_{24}H_{18}Cl_2F_{17}NO_2Ru$: C 34.02, H 2.14, N 1.65; found C 33.94, H 2.27, N 1.63.

[Ru(η^6-*p*-cymene)oxalate(1*H*,1*H*,2*H*,2*H*-perfluorodecyl-3-(pyridin-3-yl)propanoate)] 3. To a solution of [Ru(η^6-*p*-cymene)-Cl$_2$]$_2$ (0.214 g, 0.349 mmol, 1 equiv) in degassed H_2O (30 mL), silver oxalate (0.276 g, 0.907 mmol, 2.6 equiv) was added, and the resulting suspension was stirred at room temperature for 24 h. The reaction mixture was filtered on a Celite pad and washed with H_2O (2 × 30 mL) and the obtained filtrate concentrated under reduced pressure. The treated intermediate was dissolved in dichloromethane (10 mL), and a solution of the ligand **L** (0.500 g, 0.837 mmol, 2.4 equiv) was added dropwise. The resulting mixture was stirred at room temperature for 72 h. The reaction mixture was concentrated under reduced pressure almost to dryness, and a solid was precipitated with Et_2O (5 mL) and then washed successively with Et_2O (3 × 25 mL) and hexane (2 × 25 mL). A pale yellow-green solid was recovered by filtration on a frit and dried under a flow of N_2 and then under high vacuum (0.525 g, η = 82%). Mp (°C) = 181.5−183. ^{1}H NMR ($CDCl_3$) δ_H, ppm: 8.44 (1H, d, N_{py}-C$\underline{H}$-C, $^4J_{H,H}$ = 1.6 Hz), 8.36 (1H, dd overlapped, N_{py}-C$\underline{H}$-CH, $^3J_{H,H}$ = 5.7 Hz), 7.64 (1H, ddd overlapped, N_{py}-CH-C-C$\underline{H}$, $^3J_{H,H}$ = 7.8 Hz), 7.27 (1H, dd, N_{py}-CH-C$\underline{H}$, $^3J_{H,H}$ = 7.8 Hz, $^3J_{H,H}$ = 5.7 Hz), 5.48 (2H, d, 2 × CH$_3$-C-CH-C$\underline{H}$(*Ar*), $^3J_{H,H}$ = 6.1 Hz), 5.28 (2H, d, 2 × CH$_3$-C-C$\underline{H}$(*Ar*), $^3J_{H,H}$ = 6.1 Hz), 4.39 (2H, t, O-C$\underline{H_2}$-CH$_2$, $^3J_{H,H}$ = 6.4 Hz), 2.92 (2H, t, *Py*-C$\underline{H_2}$-CH$_2$-C═O, $^3J_{H,H}$ = 7.2 Hz), 2.85 (1H, sept, *Ar*-C$\underline{H}$(CH$_3$)$_2$, $^3J_{H,H}$ = 7.1 Hz), 2.66 (2H, t, *Py*-CH$_2$-C$\underline{H_2}$-C═O, $^3J_{H,H}$ = 7.2 Hz), 2.41−2.54 (2H, m, O-CH$_2$-C$\underline{H_2}$), 2.14 (3H, s, *Ar*-C$\underline{H_3}$), 1.30 (6H, d, *Ar*-CH(C$\underline{H_3}$)$_2$, $^3J_{H,H}$ = 7.1 Hz). ^{13}C NMR ($CDCl_3$) δ_C, ppm: 171.6 (1C, CH$_2$-$\underline{C}$═O), 165.3 (2C, O═$\underline{C}$-$\underline{C}$═O), 153.2 (1C, N_{py}-$\underline{C}$H-C), 151.1 (1C, N_{py}-$\underline{C}$H-CH), 138.8 (1C, N_{py}-CH-C-$\underline{C}$H), 138.5 (1C, N_{py}-CH-$\underline{C}$-CH), 125.4 (1C, N_{py}-CH-$\underline{C}$H), 105.4−121.9 (8C, m series, CH$_2$-$\underline{C}$F$_2$-CF$_2$, CH$_2$-CF$_2$-$\underline{C}$F$_2$, CH$_2$-(CF$_2$)$_2$-$\underline{C}$F$_2$, CH$_2$-(CF$_2$)$_3$-$\underline{C}$F$_2$, $\underline{C}$F$_2$-(CF$_2$)$_2$-CF$_3$, $\underline{C}$F$_2$-CF$_2$-CF$_3$, CF$_2$-$\underline{C}$F$_2$-CF$_3$, CF$_2$-CF$_2$-$\underline{C}$F$_3$), 102.3 (1C, CH$_3$-C-CH-CH-$\underline{C}$(*Ar*)), 97.0 (1C, CH$_3$-$\underline{C}$-CH(*Ar*)), 82.3 (2C, 2 × CH$_3$-C-CH-$\underline{C}$H(*Ar*)), 81.1 (2C, 2 × CH$_3$-C-$\underline{C}$H(*Ar*)), 56.8 (1C, t, O-$\underline{C}$H$_2$-CH$_2$, $^3J_{C,F}$ = 4 Hz), 34.4 (1C, *Py*-CH$_2$-$\underline{C}$H$_2$-C═O), 31.0 (1C, *Ar*-$\underline{C}$H(CH$_3$)$_2$), 30.5 (1C, t, O-CH$_2$-$\underline{C}$H$_2$, $^2J_{C,F}$ = 22 Hz), 27.6 (1C, *Py*-$\underline{C}$H$_2$-CH$_2$-C═O), 22.5 (2C, *Ar*-CH($\underline{C}$H$_3$)$_2$), 17.9 (1C, *Ar*-$\underline{C}$H$_3$). ^{19}F-NMR ($CDCl_3$) δ_F, ppm: −80.77 (3F, t, C$\underline{F_3}$, $^3J_{F,F}$ = 9.6 Hz), −113.59 (2F, m, CH$_2$-C$\underline{F_2}$-CF$_2$), −121.67 (2F, m, CH$_2$-(CF$_2$)$_2$-C$\underline{F_2}$), −121.91 (4F, m, CH$_2$-(CF$_2$)$_3$-C$\underline{F_2}$, CH$_2$-(CF$_2$)$_4$-C$\underline{F_2}$), −122.71 (2F, m, C$\underline{F_2}$-CF$_2$-CF$_3$), −123.55 (2F, m, CH$_2$-CF$_2$-C$\underline{F_2}$), −126.11 (2F, m, C$\underline{F_2}$-CF$_3$). IR (ν, cm^{-1}): 3048, 2963 (CH-*Ar*, CH$_2$, CH, CH$_3$), 1736 (C═O), 1699−1651 (oxalate-C═O), 1432−1471, (*Py* C═C, C═N), 1369, 1246−1115 (CF$_2$, CF$_3$), 1199 (C−O). ESI-MS(+): *m*/*z* found 922.0298 [M + H]$^+$, calcd for $C_{30}H_{26}F_{17}NO_6Ru$ 922.0619; the experimental isotopic pattern fits well the calculated one. Anal. (%) Calcd for $C_{30}H_{26}F_{17}NO_6Ru$: C 39.14, H 2.85, N 1.52; found C 39.17, H 2.72, N 1.50.

[Ru(η^6-benzene)oxalate(1*H*,1*H*,2*H*,2*H*-perfluorodecyl-3-(pyridin-3-yl)propanoate)] 4. To a suspension of [Ru(η^6-benzene)Cl$_2$]$_2$ (0.174 g, 0.349 mmol, 1 equiv) in degassed water (50 mL), silver oxalate (0.276 g, 0.907 mmol, 2.6 equiv) was added, and the resulting suspension was stirred at room temperature for 24 h. The reaction mixture was filtered on a Celite pad and then washed with H_2O (2 × 30 mL). The filtrate was concentrated under reduced pressure and then further dried under high vacuum. The compound was dissolved in CH_2Cl_2 (10 mL), and the ligand **L** (0.500 g, 0.837 mmol, 2.4 equiv) was added dropwise. The resulting mixture was stirred at room temperature for 72 h. The reaction mixture was filtered on a Celite pad, concentrated under reduced pressure almost to dryness. The product was precipitated with Et_2O (5 mL) and then successively washed with Et_2O (5 × 25 mL) and hexane (2 × 25 mL) and dried under high vacuum. The product was isolated as a pale yellow solid (0.126 g, η = 21%). Mp (°C): 138−139 with decomposition. ^{1}H NMR (CD_2Cl_2) δ_H, ppm: 8.50 (1H, d, N_{py}-C$\underline{H}$-C, $^4J_{H,H}$ = 1.7 Hz), 8.43 (1H, dd, N_{py}-C$\underline{H}$-CH, $^3J_{H,H}$ = 5.6 Hz, $^4J_{H,H}$ = 1.1 Hz), 7.69 (1H, ddd overlapped, N_{py}-CH-C-C$\underline{H}$, $^3J_{H,H}$ = 7.9 Hz, $^4J_{H,H}$ = 1.7 Hz), 7.33 (1H, dd, N_{py}-CH-C$\underline{H}$, $^3J_{H,H}$ = 7.7 Hz, $^3J_{H,H}$ = 5.6 Hz), 5.65 (6H, s, 6 × C$\underline{H}$(*Ar*)), 4.39 (2H, t, O-C$\underline{H_2}$-CH$_2$, $^3J_{H,H}$ = 6.4 Hz), 2.97 (2H, t, *Py*-C$\underline{H_2}$-CH$_2$-C═O, $^3J_{H,H}$ = 7.3 Hz), 2.67 (2H, t, *Py*-CH$_2$-C$\underline{H_2}$-C═O, $^3J_{H,H}$ = 7.3 Hz), 2.44−2.57 (2H, m, O-CH$_2$-C$\underline{H_2}$). ^{13}C NMR (CD_2Cl_2) δ_C, ppm: 171.9 (1C, CH$_2$-$\underline{C}$═O), 164.8 (2C, O═$\underline{C}$-$\underline{C}$═O), 153.7 (1C, N_{py}-$\underline{C}$H-C), 151.5 (1C, N_{py}-$\underline{C}$H-CH), 139.2 (1C, N_{py}-CH-C-$\underline{C}$H), 139.0 (1C, N_{py}-CH-$\underline{C}$-CH), 125.7 (1C, N_{py}-CH-$\underline{C}$H), 105.8−122.5 (8C, series of multiplets, CH$_2$-$\underline{C}$F$_2$-CF$_2$, CH$_2$-CF$_2$-$\underline{C}$F$_2$, CH$_2$-(CF$_2$)$_2$-$\underline{C}$F$_2$, CH$_2$-(CF$_2$)$_3$-$\underline{C}$F$_2$, $\underline{C}$F$_2$-(CF$_2$)$_2$-CF$_3$, $\underline{C}$F$_2$-CF$_2$-CF$_3$, CF$_2$-$\underline{C}$F$_2$-CF$_3$, CF$_2$-CF$_2$-$\underline{C}$F$_3$), 83.4 (6C, 6 × $\underline{C}$H(*Ar*)), 57.0 (1C, t, O-$\underline{C}$H$_2$-CH$_2$, $^3J_{C,F}$ = 5 Hz), 34.7 (1C, *Py*-CH$_2$-$\underline{C}$H$_2$-C═O), 30.8 (1C, t, O-CH$_2$-$\underline{C}$H$_2$, $^2J_{C,F}$ = 22 Hz), 27.9 (1C, *Py*-$\underline{C}$H$_2$-CH$_2$-C═O). ^{19}F NMR (CD_2Cl_2) δ_F, ppm: −81.10 (3F, t, C$\underline{F_3}$, $^3J_{F,F}$ = 9.9 Hz), −113.82 (2F, m, CH$_2$-C$\underline{F_2}$-CF$_2$), −121.70 (2F, m, CH$_2$-(CF$_2$)$_2$-C$\underline{F_2}$), −121.99 (4F, m, CH$_2$-(CF$_2$)$_3$-C$\underline{F_2}$, CH$_2$-(CF$_2$)$_4$-C$\underline{F_2}$), −122.88 (2F, m, C$\underline{F_2}$-CF$_2$-CF$_3$), −123.75 (2F, m, CH$_2$-CF$_2$-C$\underline{F_2}$), −126.24 (2F, m, C$\underline{F_2}$-CF$_3$). IR (ν, cm^{-1}): 3057, 2961 (CH-*Ar*, CH$_2$,CH, CH$_3$), 1739 (C═O), 1697−1645 (oxalate-C═O),1480, 1433 (*Py* C═C, C═N), 1382, 1369, 1242−1115 (CF$_2$, CF$_3$), 1197 (C−O). ESI-MS(+): *m*/*z* found 866.1707 [M + H]$^+$, calcd for $C_{26}H_{18}F_{17}NO_6Ru$, 865.9992; the experimental isotopic pattern fits well the calculated one. Anal. (%) Calcd for $C_{26}H_{18}F_{17}NO_6Ru$: C 36.12, H 2.10, N 1.62; found C 35.77, H 2.02, N 1.49.

X-ray Crystallography. The data collection of **2** and **S1** were performed at room temperature using Cu K$_\alpha$ radiation on an Agilent Technologies SuperNova dual system in combination with an Atlas CCD detector. Data reduction was carried out using CrysAlisPro.[76] The solutions and refinements were performed with SHELX.[77] The crystal structures were refined using full-matrix least-squares based on F^2 with all non-hydrogen atoms anisotropically defined. Hydrogen atoms were placed in calculated positions by means of the "riding" model. The crystal of **2** contained two independent complexes and two solvent molecules ($CHCl_3$) within the asymmetric unit. Because of the extensive disorder affecting particularly the alkyl chains, some geometrical restraints were applied to C···C distances (SADI cards used for 1,2 bonded and 1,3 nonbonded carbon atoms), to C−F bond lengths, and to F···F distances (DFIX cards employed in this case). For a better behavior of the anisotropic refinement all carbon and fluorine atoms were restrained (SIMU 0.02 card). The crystal structure of **S1** displays in its asymmetric unit one complex and one solvent molecule ($CDCl_3$). The Ru(toluene)Cl$_2$ moiety appeared to be completely

DOI: 10.1021/jm501655t
J. Med. Chem. 2015, 58, 3356−3365

disordered and was treated by the split model (occupancy for site A: 0.597(9)) in a very elegant manner (though some restraints were applied to the toluene ligand). The solvent molecule showed evident signs of disorder too, and its treatment by the split model required some restraints, applied to its geometry and displacement parameters (SADI and SIMU 0.02 cards).

Cell Culture. A2780 cells were routinely grown in RPMI-1640 medium supplemented with GlutaMAX (Gibco), containing heat-inactivated fetal calf serum (FCS, Sigma, USA) (10%) and antibiotics (penicillin (100 U/mL)/streptomycin (100 μg/mL), working concentration 1:100, BioConcept Ltd., Allschwil, Switzerland) at 37 °C and CO_2 (5%). HEK-293 and MDA-MB-231 cells were routinely grown in DMEM medium (Gibco), containing heat-inactivated FCS (10%) and antibiotics (penicillin (100 U/mL)/streptomycin (100 μg/mL), working concentration 1:100) at 37 °C and CO_2 (5%). Primary HUVECs were routinely isolated from umbilical cords. HUVECs were cultured in RPMI supplemented with 10% fetal calf serum, 10% human serum, and 1% penicillin/streptomycin (penicillin (100 U/mL)/streptomycin (100 μg/mL), working concentration 1:100) and grown in 0.2% gelatin-coated tissue culture flasks. HUVEC and ECRF24 cells were grown in gelatin-coated (0.2%) flasks containing RPMI-1640 medium supplemented with GlutaMAX (Gibco), containing heat-inactivated fetal calf serum (10%), human serum (10%), and antibiotics ((penicillin (100 U/mL)/streptomycin (100 μg/mL), working concentration 1:100) at 37 °C and CO_2 (5%).

Antiproliferative Activity in Vitro. Cytotoxicity was determined using the MTT assay (MTT = 3-(4,5-dimethyl-2-thiazolyl)-2,5-diphenyl-2*H*-tetrazolium bromide). Cells were seeded in 96-well plates as monolayers with 100 μL of cell solution per well and preincubated for 24 h in the cell medium. Compounds were prepared as DMSO solution that were rapidly dissolved in the culture medium and serially diluted to the appropriate concentration to give a final DMSO concentration of 0.5%. 100 μL of the drug solution was added to each well, and the plates were incubated for another 72 h. Subsequently, MTT (5 mg/mL solution) was added to the cells and the plates were incubated for further 4 h. The culture medium was aspirated, and the purple formazan crystals formed by the mitochondrial dehydrogenase activity of vital cells were dissolved in DMSO. The optical density, directly proportional to the number of surviving cells, was quantified at 540 nm using a multiwell plate reader, and the fraction of surviving cells was calculated from the absorbance of untreated control cells. Evaluation is based on the mean from two independent experiments, each comprising three microcultures per concentration level.

Cell Uptake Measurements. Cells were seeded in six-well plates, grown to approximately 50% confluence and incubated with the corresponding compound for 24 h. After incubation with the complex, cells were detached using an enzyme free dissociation solution (Millipore) and pelleted for 10 min at 100*g* and 4 °C and washed twice with ice cold PBS. Cell lysis was achieved using a freeze−thaw technique. All samples were analyzed for their protein content prior to ICP-MS determination using a bicinchoninic acid (BCA) assay (Sigma-Aldrich). Sample digestion was carried out in concentrated nitric acid for 3 h. Samples were then filled to a total volume of 8 mL with water. Indium was added as an internal standard at a concentration of 0.5 ppb. Determination of internalized metal content was achieved on an Elan DRC II ICP-MS instrument (PerkinElmer, Switzerland) equipped with a Meinhard nebulizer and a cyclonic spray chamber. The ICP-MS instrument was tuned using a solution provided by the manufacturer containing 1 ppb of each element Mg, In, Ce, Ba, Pb, and U. External standards were prepared gravimetrically in an identical matrix to the samples (with regard to internal standard and nitric acid) with single element standards obtained from CPI International (Amsterdam, The Netherlands).

Scratch Assay. The migration capability of cells was measured using the wound assay.[67] Human breast adenocarcinoma (MDA-MB-231) cells were grown to confluence, and cells were labeled with calcein AM (Molecular Probes, C3100MP, Carlsbad, CA, USA) for 15 min (1:2000, Molecular Probes), and "scratch wounds" (with an approximate width of 350 μm) were made in the monolayer by removing cells with a sterile scratch tool (Peira Scientific Instruments, Belgium). Cultures were washed with PBS, and the medium was replaced by fresh medium and incubated with compounds at doses between 6 and 50 μM for 14 h. Plates were scanned using an Acumen eX3 laser scanner cytometer (TTP LabTech Ltd., U.K.) to record images for computational analysis of scratch sizes using UGR Scratch Assay 6.2 software (DCI Labs, Peira Scientific Instruments, Belgium).

Apoptosis Assay. Cells were seeded on six-well plates (2×10^5 cells/well) and grown for 24 h in complete medium before treatment. Compounds **2**−**4** were freshly dissolved in DMSO, diluted in complete medium, and added to the cells at the final concentrations (IC_{50}) with a final concentration of DMSO 0.1%. After incubation for 24 h, apoptosis was measured by flow cytometric determination of subdiploid cells after DNA extraction and subsequent staining with propidium iodide (PI) as described previously.[69] Briefly, cells were harvested and subsequently fixed in 70% ethanol at 20 °C. After 2 h, the cells were resuspended in DNA extraction buffer (45 mM Na_2HPO_4, 2.5 mM citric acid, and 1% Triton X-100, pH 7.4) for 20 min at 37 °C. PI was added to a final concentration of 20 μg/mL, and log scale red fluorescence was analyzed using a FACS Calibur (BD Biosciences, NJ, USA).

CAM Model. The in vivo experiments were performed in accordance with ethical regulations in Swiss law under the guidance of the local institution authority. Antiangiogenic efficacy of **2**−**4** was tested in the physiologically developing chicken embryo chorioallantoic membrane (CAM) model[70] between embryo development days (EDDs) 11 and 14. Complexes **2**−**4** were applied by iv injection (50 μM, 80 μL/day for 4 consecutive days) at EDDs 11, 12, 13, and 14. The control eggs were treated with 80 μL/day of 0.9% NaCl for 4 consecutive days). At EDD 15, the CAMs were visualized in ovo using FITC−dextran (20 kDa, 20 μL, 25 mg/mL, Sigma-Aldrich) epi-fluorescence angiography and subsequently analyzed by the image-processing quantification method described previously.[71] Briefly, on the basis of the FITC−dextran fluorescence angiography, the skeleton of the vascular network is built, and defined descriptors, i.e., branching points (mm^2), give information on the vascular architecture. At least five eggs were tested per condition. Error bars represent the standard error of the mean.

Statistical Analysis. Values are given as mean values ± standard deviations (in vitro) or the standard error of the mean (in vivo). Data are represented as averages of independent experiments. Statistical analysis for cell uptake was done using the pairwise *t*-test with Bonferroni adjustment, confirmed by the Tukey HSD multiple testing. Statistical analysis was done using the *t*-test (CAM). The *p-values lower than 0.05 were considered statistically significant (**p-value of <0.01).

■ ASSOCIATED CONTENT

Ⓢ Supporting Information

Additional figures illustrating X-ray structure of complex **S1**, crystallographic data for **2** and **S1**, packing in the crystal of **2**, packing in the crystal of **S1**, and crystallographic information. CCDC reference numbers 1057230 and 1057231 contain the supplementary crystallographic data for the X-ray studies reported in this paper. These data can be obtained free of charge at www.ccdc.cam.ac.uk/conts/retrieving.html or from the Cambridge Crystallographic Data Centre, e-mail: deposit@ccdc.cam.ac.uk. This material is available free of charge via the Internet at http://pubs.acs.org.

■ AUTHOR INFORMATION

Corresponding Author

*Phone: +41216939854. E-mail: paul.dyson@epfl.ch.

Notes

The authors declare no competing financial interest.

DOI: 10.1021/jm501655t
J. Med. Chem. 2015, 58, 3356−3365

■ ACKNOWLEDGMENTS

We thank the Swiss National Science Foundation (C.M.C.), State Secretariat for Education, Research and Innovation SERI (to P.N.-S.), and EPFL for financial support and Euro Solari for the elemental analysis and the help provided to obtain the crystal structures.

■ ABBREVIATIONS USED

CAM, chorioallantoic membrane; DMSO, dimethyl sulfoxide; FITC−dextran, fluorescein isothiocyanate−dextran (20 kDa); PI, propidium iodide

■ REFERENCES

(1) Ohmichi, M.; Hayakawa, J.; Tasaka, K.; Kurachi, H.; Murata, Y. Mechanisms of platinum drug resistance. *Trends Pharmacol. Sci.* **2005**, *26*, 113−116.
(2) Cooke, S. L.; Brenton, J. D. Evolution of platinum resistance in high-grade serous ovarian cancer. *Lancet Oncol.* **2011**, *12*, 1169−1174.
(3) Wang, D.; Lippard, S. J. Cellular processing of platinum anticancer drugs. *Nat. Rev. Drug Discovery* **2005**, *4*, 307−320.
(4) Reedijk, J. New clues for platinum antitumor chemistry: Kinetically controlled metal binding to DNA. *Proc. Natl. Acad. Sci. U.S.A.* **2003**, *100*, 3611−3616.
(5) Jamieson, E. R.; Lippard, S. J. Structure, recognition, and processing of cisplatin-DNA adducts. *Chem. Rev.* **1999**, *99*, 2467−2498.
(6) van Zutphen, S.; Reedijk, J. Targeting platinum anti-tumour drugs: Overview of strategies employed to reduce systemic toxicity. *Coord. Chem. Rev.* **2005**, *249*, 2845−2853.
(7) Yao, X.; Panichpisal, K.; Kurtzman, N.; Nugent, K. Cisplatin nephrotoxicity: a review. *Am. J. Med. Sci.* **2007**, *334*, 115−124.
(8) Cubeddu, L. X.; Hoffmann, I. S.; Fuenmayor, N. T.; Finn, A. L. Efficacy of ondansetron (GR 38032F) and the role of serotonin in cisplatin-induced nausea and vomiting. *N. Engl. J. Med.* **1990**, *322*, 810−816.
(9) Sanchez-Gonzalez, P. D.; Lopez-Hernandez, F. J.; Lopez-Novoa, J. M.; Morales, A. I. An integrative view of the pathophysiological events leading to cisplatin nephrotoxicity. *Crit. Rev. Toxicol.* **2011**, *41*, 803−821.
(10) Chin, C. F.; Yap, S. Q.; Li, J.; Pastorin, G.; Ang, W. H. Ratiometric delivery of cisplatin and doxorubicin using tumour-targeting carbon-nanotubes entrapping platinum(IV) prodrugs. *Chem. Sci.* **2014**, *5*, 2265−2270.
(11) Min, Y.; Mao, C.-Q.; Chen, S.; Ma, G.; Wang, J.; Liu, Y. Combating the drug resistance of cisplatin using a platinum prodrug based delivery system. *Angew. Chem., Int. Ed.* **2012**, *51*, 6742−6747.
(12) Wang, X.; Guo, Z. Targeting and delivery of platinum-based anticancer drugs. *Chem. Soc. Rev.* **2013**, *42*, 202−224.
(13) Bruijnincx, P. C. A.; Sadler, P. J. New trends for metal complexes with anticancer activity. *Curr. Opin. Chem. Biol.* **2008**, *12*, 197−206.
(14) Fricker, S. P. Metal based drugs: from serendipity to design. *Dalton Trans.* **2007**, 4903−4917.
(15) Hartinger, C. G.; Metzler-Nolte, N.; Dyson, P. J. Challenges and opportunities in the development of organometallic anticancer drugs. *Organometallics* **2012**, *31*, 5677−5685.
(16) Bergamo, A.; Sava, G. Ruthenium anticancer compounds: myths and realities of the emerging metal-based drugs. *Dalton Trans.* **2011**, *40*, 7817−7823.
(17) Weiss, A.; Berndsen, B. H.; Dubois, M.; Müller, M.; Schibli, R.; Griffioen, A. W.; Dyson, P. J.; Nowak-Sliwinska, P. In vivo anti-tumor activity of the organometallic ruthenium(II)-arene complex [Ru(η6-p-cymene)Cl2(pta)] (RAPTA-C) in human ovarian and colorectal carcinomas. *Chem. Sci.* **2014**, *5*, 4742−4748.
(18) Bergamo, A.; Gagliardi, R.; Scarcia, V.; Furlani, A.; Alessio, E.; Mestroni, G.; Sava, G. In vitro cell cycle arrest, in vivo action on solid metastasizing tumors, and host toxicity of the antimetastatic drug NAMI-A and cisplatin. *J. Pharmacol. Exp. Ther.* **1999**, *289*, 559−564.
(19) Guo, W.; Zheng, W.; Luo, Q.; Li, X.; Zhao, Y.; Xiong, S.; Wang, F. Transferrin serves as a mediator to deliver organometallic ruthenium(II) anticancer complexes into cells. *Inorg. Chem.* **2013**, *52*, 5328−5338.
(20) Mendoza-Ferri, M. G.; Hartinger, C. G.; Mendoza, M. A.; Groessl, M.; Egger, A. E.; Eichinger, R. E.; Mangrum, J. B.; Farrell, N. P.; Maruszak, M.; Bednarski, P. J.; Klein, F.; Jakupec, M. A.; Nazarov, A. A.; Severin, K.; Keppler, B. K. Transferring the concept of multinuclearity to ruthenium complexes for improvement of anticancer activity. *J. Med. Chem.* **2009**, *52*, 916−925.
(21) Rademaker-Lakhai, J. M.; van den Bongard, D.; Pluim, D.; Beijnen, J. H.; Schellens, J. H. M. A phase I and pharmacological study with imidazolium-*trans*-DMSO-imidazole-tetrachlororuthenate, a novel ruthenium anticancer agent. *Clin. Cancer Res.* **2004**, *10*, 3717−3727.
(22) Hartinger, C. G.; Jakupec, M. A.; Zorbas-Seifried, S.; Groessl, M.; Egger, A.; Berger, W.; Zorbas, H.; Dyson, P. J.; Keppler, B. K. KP1019, a new redox-active anticancer agent—preclinical development and results of a clinical phase I study in tumor patients. *Chem. Biodiversity* **2008**, *5*, 2140−2155.
(23) Trondl, R.; Heffeter, P.; Kowol, C. R.; Jakupec, M. A.; Berger, W.; Keppler, B. K. NKP-1339, the first ruthenium-based anticancer drug on the edge to clinical application. *Chem. Sci.* **2014**, *5*, 2925−2932.
(24) Yan, Y. K.; Melchart, M.; Habtemariam, A.; Sadler, P. J. Organometallic chemistry, biology and medicine: ruthenium arene anticancer complexes. *Chem. Commun.* **2005**, 4764−4776.
(25) Clarke, M. J.; Bitler, S.; Rennert, D.; Buchbinder, M.; Kelman, A. D. Reduction and subsequent binding of ruthenium ions catalyzed by subcellular components. *J. Inorg. Biochem.* **1980**, *12*, 79−87.
(26) Jakupec, M. A.; Reisner, E.; Eichinger, A.; Pongratz, M.; Arion, V. B.; Galanski, M.; Hartinger, C. G.; Keppler, B. K. Redox-active antineoplastic ruthenium complexes with indazole: correlation of in vitro potency and reduction potential. *J. Med. Chem.* **2005**, *48*, 2831−2837.
(27) Ang, W. H.; Casini, A.; Sava, G.; Dyson, P. J. Organometallic ruthenium-based antitumor compounds with novel modes of action. *J. Organomet. Chem.* **2011**, *696*, 989−998.
(28) Ang, W. H.; Daldini, E.; Scolaro, C.; Scopelliti, R.; Juillerat-Jeannerat, L.; Dyson, P. J. Development of organometallic ruthenium-arene anticancer drugs that resist hydrolysis. *Inorg. Chem.* **2006**, *45*, 9006−9013.
(29) Scolaro, C.; Bergamo, A.; Brescacin, L.; Delfino, R.; Cocchietto, M.; Laurenczy, G.; Geldbach, T. J.; Sava, G.; Dyson, P. J. In vitro and in vivo evaluation of ruthenium(II)-arene PTA complexes. *J. Med. Chem.* **2005**, *48*, 4161−4171.
(30) Bergamo, A.; Masi, A.; Dyson, P. J.; Sava, G. Modulation of the metastatic progression of breast cancer with an organometallic ruthenium compound. *Int. J. Oncol.* **2008**, *33*, 1281−1289.
(31) Bergamo, A.; Gaiddon, C.; Schellens, J. H. M.; Beijnen, J. H.; Sava, G. Approaching tumour therapy beyond platinum drugs: status of the art and perspectives of ruthenium drug candidates. *J. Inorg. Biochem.* **2012**, *106*, 90−99.
(32) Nowak-Sliwinska, P.; van Beijnum, J. R.; Casini, A.; Nazarov, A. A.; Wagnières, G.; van den Bergh, H.; Dyson, P. J.; Griffioen, A. W. Organometallic ruthenium(II) arene compounds with antiangiogenic activity. *J. Med. Chem.* **2011**, *54*, 3895−3902.
(33) Chatterjee, S.; Kundu, S.; Bhattacharyya, A.; Hartinger, C. G.; Dyson, P. J. The ruthenium(II)-arene compound RAPTA-C induces apoptosis in EAC cells through mitochondrial and p53-JNK pathways. *J. Biol. Inorg. Chem.* **2008**, *13*, 1149−1155.
(34) Adhireksan, Z.; Davey, G. E.; Campomanes, P.; Groessl, M.; Clavel, C. M.; Yu, H.; Nazarov, A. A.; Yeo, C. H.; Ang, W. H.; Droge, P.; Rothlisberger, U.; Dyson, P. J.; Davey, C. A. Ligand substitutions between ruthenium-cymene compounds can control protein versus DNA targeting and anticancer activity. *Nat. Commun.* **2014**, *5*, 3462.

DOI: 10.1021/jm501655t
J. Med. Chem. 2015, 58, 3356−3365

(35) Wu, B.; Ong, M. S.; Groessl, M.; Adhireksan, Z.; Hartinger, C. G.; Dyson, P. J.; Davey, C. A. A ruthenium antimetastasis agent forms specific histone protein adducts in the nucleosome core. *Chem.—Eur. J.* **2011**, *17*, 3562−3566.
(36) Qian, D. Z.; Kato, Y.; Shabbeer, S.; Wei, Y.; Verheul, H. M.; Salumbides, B.; Sanni, T.; Atadja, P.; Pili, R. Targeting tumor angiogenesis with histone deacetylase inhibitors: the hydroxamic acid derivative LBH589. *Clin. Cancer Res.* **2006**, *12*, 634−642.
(37) Kim, M. S.; Kwon, H. J.; Lee, Y. M.; Baek, J. H.; Jang, J. E.; Lee, S. W.; Moon, E. J.; Kim, H. S.; Lee, S. K.; Chung, H. Y.; Kim, C. W.; Kim, K. W. Histone deacetylases induce angiogenesis by negative regulation of tumor suppressor genes. *Nat. Med.* **2001**, *7*, 437−443.
(38) Hufziger, K. T.; Thowfeik, F. S.; Charboneau, D. J.; Nieto, I.; Dougherty, W. G.; Kassel, W. S.; Dudley, T. J.; Merino, E. J.; Papish, E. T.; Paul, J. J. Ruthenium dihydroxybipyridine complexes are tumor activated prodrugs due to low pH and blue light induced ligand release. *J. Inorg. Biochem.* **2014**, *130*, 103−111.
(39) Renfrew, A. K.; Phillips, A. D.; Tapavicza, E.; Scopelliti, R.; Rothlisberger, U.; Dyson, P. J. Tuning the efficacy of ruthenium(II)-arene (RAPTA) antitumor compounds with fluorinated arene ligands. *Organometallics* **2009**, *28*, 5061−5071.
(40) Yadav, A.; Janaratne, T.; Krishnan, A.; Singhal, S. S.; Yadav, S.; Dayoub, A. S.; Hawkins, D. L.; Awasthi, S.; MacDonnell, F. M. Regression of lung cancer by hypoxia-sensitizing ruthenium polypyridyl complexes. *Mol. Cancer Ther.* **2013**, *12*, 643−653.
(41) Baban, D. F.; Seymour, L. W. Control of tumour vascular permeability. *Adv. Drug Delivery Rev.* **1998**, *34*, 109−119.
(42) Modi, S.; Jain, J. P.; Domb, A. J.; Kumar, N. Exploiting EPR in polymer drug conjugate delivery for tumor targeting. *Curr. Pharm. Des.* **2006**, *12*, 4785−4796.
(43) Govender, P.; Antonels, N. C.; Mattsson, J.; Renfrew, A. K.; Dyson, P. J.; Moss, J. R.; Therrien, B.; Smith, G. S. Anticancer activity of multinuclear arene ruthenium complexes coordinated to dendritic polypyridyl scaffolds. *J. Organomet. Chem.* **2009**, *694*, 3470−3476.
(44) Govender, P.; Renfrew, A. K.; Clavel, C. M.; Dyson, P. J.; Therrien, B.; Smith, G. S. Antiproliferative activity of chelating *N,O*- and *N,N*-ruthenium(II) arene functionalised poly(propyleneimine) dendrimer scaffolds. *Dalton Trans.* **2011**, *40*, 1158−1167.
(45) Govender, P.; Sudding, L. C.; Clavel, C. M.; Dyson, P. J.; Therrien, B.; Smith, G. S. The influence of RAPTA moieties on the antiproliferative activity of peripheral-functionalised poly(salicylaldiminato) metallodendrimers. *Dalton Trans.* **2013**, *42*, 1267−1277.
(46) Furrer, M. A.; Schmitt, F.; Wiederkehr, M.; Juillerat-Jeanneret, L.; Therrien, B. Cellular delivery of pyrenyl-arene ruthenium complexes by a water-soluble arene ruthenium metalla-cage. *Dalton Trans.* **2012**, *41*, 7201−7211.
(47) Blunden, B. M.; Thomas, D. S.; Stenzel, M. H. Macromolecular ruthenium complexes as anti-cancer agents. *Polym. Chem.* **2012**, *3*, 2964−2975.
(48) Blunden, B. M.; Lu, H. X.; Stenzel, M. H. Enhanced delivery of the RAPTA-C macromolecular chemotherapeutic by conjugation to degradable polymeric micelles. *Biomacromolecules* **2013**, *14*, 4177−4188.
(49) Therrien, B.; Suss-Fink, G.; Govindaswamy, P.; Renfrew, A. K.; Dyson, P. J. The "complex-in-a-complex" cations [(acac)(2)M subset of RU6(p-iPrC(6)H(4)Me)(6)(tpt)(2)(dhbq)(3)](6+): a Trojan horse for cancer cells. *Angew. Chem., Int. Ed.* **2008**, *47*, 3773−3776.
(50) Renfrew, A. K.; Scopelliti, R.; Dyson, P. J. Use of perfluorinated phosphines to provide thermomorphic anticancer complexes for heat-based tumor targeting. *Inorg. Chem.* **2010**, *49*, 2239−2246.
(51) Clavel, C. M.; Paunescu, E.; Nowak-Sliwinska, P.; Dyson, P. J. Thermoresponsive organometallic arene ruthenium complexes for tumour targeting. *Chem. Sci.* **2014**, *5*, 1097−1101.
(52) Bergamini, P.; Marvelli, L.; Marchi, A.; Vassanelli, F.; Fogagnolo, M.; Formaglio, P.; Bernardi, T.; Gavioli, R.; Sforza, F. Platinum and ruthenium complexes of new long-tail derivatives of PTA (1,3,5-triaza-7-phosphaadamantane): Synthesis, characterization and antiproliferative activity on human tumoral cell lines. *Inorg. Chim. Acta* **2012**, *391*, 162−170.
(53) Renfrew, A. K.; Juillerat-Jeanneret, L.; Dyson, P. J. Adding diversity to ruthenium(II)-arene anticancer (RAPTA) compounds via click chemistry: The influence of hydrophobic chains. *J. Organomet. Chem.* **2011**, *696*, 772−779.
(54) Khan, F. A.; Therrien, B.; Suss-Fink, G.; Zava, O.; Dyson, P. J. Arene ruthenium dichloro complexes containing isonicotinic ester ligands: Synthesis, molecular structure and cytotoxicity. *J. Organomet. Chem.* **2013**, *730*, 49−56.
(55) Suss-Fink, G.; Khan, F. A.; Juillerat-Jeanneret, L.; Dyson, P. J.; Renfrew, A. K. Synthesis and anticancer activity of long-chain isonicotinic ester ligand-containing arene ruthenium complexes and nanoparticles. *J. Cluster Sci.* **2010**, *21*, 313−324.
(56) Clavel, C. M.; Paunescu, E.; Nowak-Sliwinska, P.; Griffioen, A. W.; Scopelliti, R.; Dyson, P. J. Discovery of a highly tumor-selective organometallic ruthenium(II)-arene complex. *J. Med. Chem.* **2014**, *57*, 3546−3558.
(57) Renfrew, A. K.; Phillips, A. D.; Egger, A. E.; Hartinger, C. G.; Bosquain, S. S.; Nazarov, A. A.; Keppler, B. K.; Gonsalvi, L.; Peruzzini, M.; Dyson, P. J. Influence of structural variation on the anticancer activity of RAPTA-type complexes: ptn versus pta. *Organometallics* **2009**, *28*, 1165−1172.
(58) Wang, F. Y.; Habtemariam, A.; van der Geer, E. P. L.; Fernandez, R.; Melchart, M.; Deeth, R. J.; Aird, R.; Guichard, S.; Fabbiani, F. P. A.; Lozano-Casal, P.; Oswald, I. D. H.; Jodrell, D. I.; Parsons, S.; Sadler, P. J. Controlling ligand substitution reactions of organometallic complexes: Tuning cancer cell cytotoxicity. *Proc. Natl. Acad. Sci. U.S.A.* **2005**, *102*, 18269−18274.
(59) Habtemariam, A.; Melchart, M.; Fernandez, R.; Parsons, S.; Oswald, I. D.; Parkin, A.; Fabbiani, F. P.; Davidson, J. E.; Dawson, A.; Aird, R. E.; Jodrell, D. I.; Sadler, P. J. Structure-activity relationships for cytotoxic ruthenium(II) arene complexes containing N,N-, N,O-, and O,O-chelating ligands. *J. Med. Chem.* **2006**, *49*, 6858−6868.
(60) Scolaro, C.; Hartinger, C. G.; Allardyce, C. S.; Keppler, B. K.; Dyson, P. J. Hydrolysis study of the bifunctional antitumour compound RAPTA-C, [Ru(eta6-p-cymene)Cl2(pta)]. *J. Inorg. Biochem.* **2008**, *102*, 1743−1748.
(61) Di Pasqua, A. J.; Kerwood, D. J.; Shi, Y.; Goodisman, J.; Dabrowiak, J. C. Stability of carboplatin and oxaliplatin in their infusion solutions is due to self-association. *Dalton Trans.* **2011**, *40*, 4821−4825.
(62) Pavelka, M.; Lucas, M. F. A.; Russo, N. On the hydrolysis mechanism of the second-generation anticancer drug carboplatin. *Chem.—Eur. J.* **2007**, *13*, 10108−10116.
(63) Kilpin, K. J.; Cammack, S. M.; Clavel, C. M.; Dyson, P. J. Ruthenium(II) arene PTA (RAPTA) complexes: impact of enantiomerically pure chiral ligands. *Dalton Trans.* **2013**, *42*, 2008−2014.
(64) Hanif, M.; Meier, S. M.; Kandioller, W.; Bytzek, A.; Hejl, M.; Hartinger, C. G.; Nazarov, A. A.; Arion, V. B.; Jakupec, M. A.; Dyson, P. J.; Keppler, B. K. From hydrolytically labile to hydrolytically stable Ru(II)-arene anticancer complexes with carbohydrate-derived co-ligands. *J. Inorg. Biochem.* **2011**, *105*, 224−231.
(65) Hanif, M.; Nazarov, A. A.; Hartinger, C. G.; Kandioller, W.; Jakupec, M. A.; Arion, V. B.; Dyson, P. J.; Keppler, B. K. Osmium(II)—versus ruthenium(II)—arene carbohydrate-based anticancer compounds: similarities and differences. *Dalton Trans.* **2010**, *39*, 7345−7352.
(66) Allardyce, C. S.; Dyson, P. J.; Ellis, D. J.; Heath, S. L. [Ru(eta(6)-p-cymene)Cl-2(pta)] (pta=1,3,5-triaza-7-phosphatricyclo-[3.3.1.1]decane): a water soluble compound that exhibits pH dependent DNA binding providing selectivity for diseased cells. *Chem. Commun.* **2001**, 1396−1397.
(67) Weiss, A.; van Beijnum, J. R.; Bonvin, D.; Jichlinski, P.; Dyson, P. J.; Griffioen, A. W.; Nowak-Sliwinska, P. Low-dose angiostatic tyrosine kinase inhibitors improve photodynamic therapy for cancer: lack of vascular normalization. *J. Cell. Mol. Med.* **2014**, *18*, 480−491.

DOI: 10.1021/jm501655t
J. Med. Chem. 2015, 58, 3356−3365

(68) Holliday, D. L.; Speirs, V. Choosing the right cell line for breast cancer research. *Breast Cancer Res.* **2011**, *13*, 215.
(69) Nazarov, A. A.; Baquie, M.; Nowak-Sliwinska, P.; Zava, O.; van Beijnum, J. R.; Groessl, M.; Chisholm, D. M.; Ahmadi, Z.; McIndoe, J. S.; Griffioen, A. W.; van den Bergh, H.; Dyson, P. J. Synthesis and characterization of a new class of anti-angiogenic agents based on ruthenium clusters. *Sci. Rep.* **2013**, *3*, 1485.
(70) Nowak-Sliwinska, P.; Segura, T.; Iruela-Arispe, M. L. The chicken chorioallantoic membrane model in biology, medicine and bioengineering. *Angiogenesis* **2014**, *17*, 779−804.
(71) Nowak-Sliwinska, P.; Ballini, J. P.; Wagnieres, G.; van den Bergh, H. Processing of fluorescence angiograms for the quantification of vascular effects induced by anti-angiogenic agents in the CAM model. *Microvasc. Res.* **2010**, *79*, 21−28.
(72) Morbidelli, L.; Donnini, S.; Filippi, S.; Messori, L.; Piccioli, F.; Orioli, P.; Sava, G.; Ziche, M. Antiangiogenic properties of selected ruthenium(III) complexes that are nitric oxide scavengers. *Br. J. Cancer* **2003**, *88*, 1484−1491.
(73) Vacca, A.; Bruno, M.; Boccarelli, A.; Coluccia, M.; Ribatti, D.; Bergamo, A.; Garbisa, S.; Sartor, L.; Sava, G. Inhibition of endothelial cell functions and of angiogenesis by the metastasis inhibitor NAMI-A. *Br. J. Cancer* **2002**, *86*, 993−998.
(74) Bennett, M. A.; Smith, A. K. Arene ruthenium(II) complexes formed by dehydrogenation of cyclohexadienes with ruthenium(III) trichloride. *J. Chem. Soc. Dalton* **1974**, 233−241.
(75) Fulmer, G. R.; Miller, A. J. M.; Sherden, N. H.; Gottlieb, H. E.; Nudelman, A.; Stoltz, B. M.; Bercaw, J. E.; Goldberg, K. I. NMR chemical shifts of trace impurities: common laboratory solvents, organics, and gases in deuterated solvents relevant to the organometallic chemist. *Organometallics* **2010**, *29*, 2176−2179.
(76) *CrysAlisPro*, version 1.171.37.31; Agilent Technologies: Santa Clara, CA, 2014.
(77) Sheldrick, G. M. A short history of SHELX. *Acta Crystallogr. A* **2008**, *64*, 112−122.

DOI: 10.1021/jm501655t
J. Med. Chem. 2015, 58, 3356−3365